
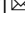


## Continuous quantum light from a dark atom

Karl Nicolas Tolazzi<sup>1</sup>  , Bo Wang<sup>1</sup>, Christopher Ianzano<sup>1</sup>, Jonas Neumeier<sup>1</sup>, Celso Jorge Villas-Boas<sup>2</sup> & Gerhard Rempe<sup>1</sup>

Cycling processes are important in many areas of physics ranging from lasers to topological insulators, often offering surprising insights into dynamical and structural aspects of the respective system. Here we report on a quantum-nonlinear wave-mixing experiment where resonant lasers and an optical cavity define a closed cycle between several ground and excited states of a single atom. We show that, for strong atom-cavity coupling and steady-state driving, the entanglement between the atomic states and intracavity photon number suppresses the excited-state population via quantum interference, effectively reducing the cycle to the atomic ground states. The system dynamics then result from transitions within a harmonic ladder of entangled dark states, one for each cavity photon number, and a quantum Zeno blockade that generates antibunching in the photons emitted from the cavity. The reduced cycle suppresses unwanted optical pumping into atomic states outside the cycle, thereby enhancing the number of emitted photons.

<sup>1</sup>Max-Planck-Institut für Quantenoptik, Hans-Kopfermann-Str. 1, Garching, Germany. <sup>2</sup>Departamento de Física, Universidade Federal de São Carlos, São Carlos, Brazil. ✉email: [nicolas.tolazzi@mpq.mpg.de](mailto:nicolas.tolazzi@mpq.mpg.de)

When two light fields resonantly drive transitions from two different atomic ground states to a common excited state, forming a three-level lambda-type system, the quantum-mechanical transition amplitudes to that state can interfere destructively. This inhibits excitation and produces a superposition between the two ground states, called a dark state<sup>1</sup>. Dark states give rise to electromagnetically induced transparency<sup>2</sup> and slow light<sup>3</sup>, appear in lasing without inversion<sup>4</sup>, are employed for producing<sup>5</sup> and storing<sup>6</sup> single photons in quantum networks<sup>7,8</sup>, and are widely used in physics and chemistry in the form of a stimulated Raman adiabatic passage<sup>9</sup>.

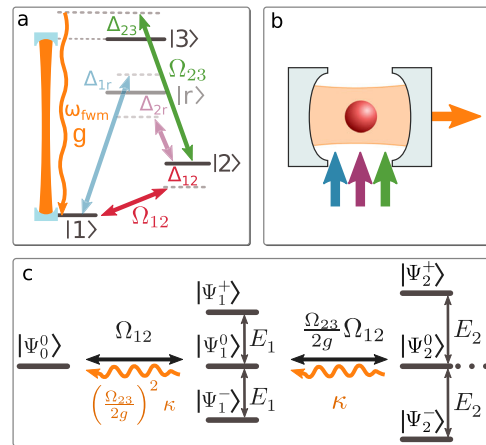
The main advantage of such dark states is that they protect the system from decoherence related to the excited state. They are thus ideal for continuous experiments with atomic cycling currents involving the excited state, as the removal of the decay channel allows the cycle to run for a longer period. Unfortunately, attempting to close the lambda system and generating a cycling current with a third field that directly couples the two ground states results in the destruction of the dark state, except in the restricting case when both driving strengths of the lambda subsystem are equal<sup>10</sup>. In general, the breakdown of the dark state in such a system brings population to the excited atomic state. Thus, decoherence is reintroduced via atomic decay and additional loss channels are opened via depumping to, e.g., states outside the cycle.

As we report here, this breakdown can be mitigated by replacing one of the coherent driving fields of the closed cycle by an optical cavity strongly coupled to the corresponding atomic transition. In this case the entanglement of the atomic ground states with the photon number in the cavity effectively preserves the destructive interference of atomic excitation amplitudes, and thus, the dark states. The possibility to have any number of photons in the cavity furthermore produces an infinite harmonic ladder of dark states that can be used to produce either quantum or coherent light<sup>11</sup>. Replacing a laser with a cavity has the further advantage that it introduces in the otherwise decoherence-free subspace in which the system operates, a well-defined dissipation channel through which the system dynamics can be observed in real time.

## Results and discussion

Our system consists of a single <sup>87</sup>Rb atom strongly coupled to a high-finesse optical Fabry-Pérot resonator. Our parameters are  $(\kappa, \gamma, g)/2\pi = (1.5, 3.0, 10.2)$  MHz, with  $\kappa$  the cavity-field decay rate,  $\gamma$  the atomic polarization decay rate, and  $g$  the atom-cavity coupling constant. This  $g$  is the maximum value and varies slightly between atoms at different trapping positions within the cavity. The condition  $(\kappa, \gamma) \ll g$  puts the system well into the strong-coupling regime of cavity quantum electrodynamics (CQED).

Figure 1a shows the relevant level scheme of the atom together with the driven transitions. Two ground states  $|1\rangle = |5S_{1/2}, F = 1, m_F = 1\rangle$  and  $|2\rangle = |5S_{1/2}, F = 2, m_F = 2\rangle$  are connected via a Raman transition with intermediate state  $|r\rangle$  which is a virtual level close to the  $D_1$  line of Rubidium (with detuning  $\approx 4.5$  GHz). The cavity is resonant with the transition  $|1\rangle \leftrightarrow |3\rangle = |5P_{3/2}, F = 2, m_F = 2\rangle$ . In the experiment, the transitions  $|1\rangle \leftrightarrow |r\rangle$ ,  $|2\rangle \leftrightarrow |r\rangle$  and  $|2\rangle \leftrightarrow |3\rangle$  are addressed by lasers with frequencies  $\omega_{1r}$ ,  $\omega_{2r}$  and  $\omega_{23}$  respectively, all of them illuminating the atom. Together with the transition driven by the vacuum field of the cavity, this forms a closed cycle where new light with frequency  $\omega_{fwm}$  is continuously generated and emitted from the cavity. The geometric setup of the system is depicted in Fig. 1b. The scheme can be seen as a double-lambda or butterfly system (a typical system capable of four-wave mixing processes<sup>12,13</sup>) where



**Fig. 1 System description.** **a** The atomic level scheme with ground states  $|1\rangle$  and  $|2\rangle$ , the intermediate virtual state  $|r\rangle$  and excited state  $|3\rangle$ . The atom is strongly coupled to the cavity (orange) which is resonant to the transition from  $|1\rangle$  to  $|3\rangle$ . The system is driven by three lasers with detunings  $\Delta_{1r}$ ,  $\Delta_{2r}$ ,  $\Delta_{23}$  to their respective excited states. A new field with frequency  $\omega_{fwm}$  is generated. **b** A sketch of the experimental setup including the atom, cavity and light fields that drive the atom. **c** The effective level scheme that forms for  $\Omega_{12} \ll (\Omega_{23}, g)$ , with  $\Omega_{ij}$  being the Rabi frequency of the laser drive between state  $|i\rangle$  and state  $|j\rangle$  with  $i, k \in 1, 2, 3$ . The dark state transitions are depicted with their effective driving strength and their decay rates in the limit of  $\Omega_{23} \ll g$ .  $|\Psi_n^{0,+,-}\rangle$  represents the dark states as defined in the main text,  $\kappa$  the cavity-field decay rate and  $g$  the coupling constant.

the two lambda subsystems share ground states. As the Raman transition is far off-resonant we can assume a simplified level scheme where the transition between levels  $|1\rangle$  and  $|2\rangle$  is resonantly driven with Rabi frequency  $\Omega_{12}$  and the state  $|r\rangle$  is eliminated. A discussion of the full Hamiltonian and simulations can be found as Note 1 in the Supplementary Information.

**Effective level scheme.** For all fields resonant and  $\Omega_{12} = 0$ , the eigenstates of the system form a ladder of triplets (except for the lowest state) (see Fig. 1c), as in cavity electromagnetically induced transparency<sup>14–17</sup>. These states then read

$$|\Psi_0^0\rangle = |1, 0\rangle \quad (1)$$

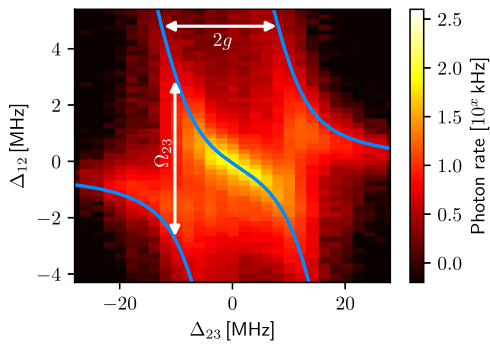
for zero photons and

$$|\Psi_n^0\rangle \propto \frac{\Omega_{23}}{2} |1, n\rangle - g\sqrt{n} |2, n-1\rangle, \quad (2)$$

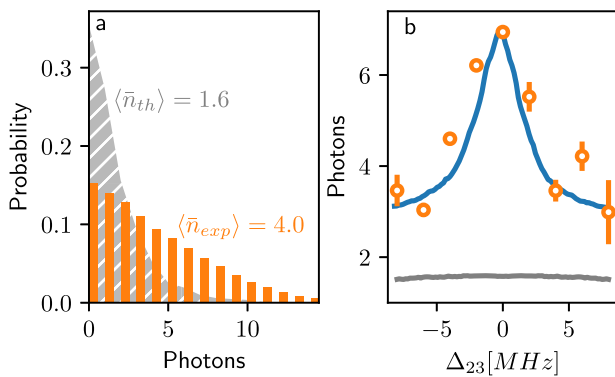
$$|\Psi_n^\pm\rangle \propto g\sqrt{n} |1, n\rangle + \frac{\Omega_{23}}{2} |2, n-1\rangle \pm E_n |3, n-1\rangle, \quad (3)$$

with  $E_n = \sqrt{ng^2 + \Omega_{23}^2/4}$  for  $n$  photons. Here the bare states are of the form  $|\text{atomic state, photon number}\rangle$ , and  $\Omega_{23}$  is the Rabi frequency of the transition  $|2\rangle \leftrightarrow |3\rangle$ . The states  $|\Psi_n^\pm\rangle$  are superposition states with both atomic and cavity excitation and have an energy splitting of  $E_n$ . The states  $|\Psi_n^0\rangle$  are dark states with no contribution from the excited atomic state,  $|3\rangle$ , exhibiting atom-cavity entanglement for  $n > 0$ . For  $\Omega_{12} \ll (g, \Omega_{23}, \kappa)$ , as in our experiment, the coherent Raman-laser driving can be treated as a perturbation.

The eigenenergies of the system can be measured by driving transitions from the ground state to these dressed eigenstates. Only when the driving fields resonantly excite an eigenstate of the first (or higher) manifold, the system exhibits a nonzero cavity photon number and photons leave the cavity. Figure 2 shows the photon emission rate from the cavity when performing a two-



**Fig. 2 System spectroscopy.** The emitted rate of photons from the cavity versus the detunings  $\Delta_{12}$  and  $\Delta_{23}$  in logarithmic scale. The blue lines in the figure are the theoretically calculated energies of the one-photon states for the ideal system. Also marked are the splittings between these eigenenergies, which are  $2g$  in horizontal and  $\Omega_{23}$  in the vertical direction. The experimental Rabi frequencies are  $\Omega_{23}/2\pi = 4.0$  MHz and  $\Omega_{12}/2\pi = 0.4$  MHz with a coupling constant  $g/2\pi = 10.2$  MHz.



**Fig. 3 Photon generation from a dark state.** **a** The photon-number probability distribution (orange) measured for zero detuning ( $\Delta_{23} = \Delta_{12} = 0$ ) and a  $60 \mu\text{s}$  long observation interval. As a comparison, a quantum simulation was performed to find the expected photon-number distribution (gray curve in background) from a free-space atom interacting with the same driving fields.  $\bar{n}$  means the average photon number. **b** The experimentally measured number of photons (orange), extrapolated to infinite measurement time as a function of  $\Delta_{23}$ . The curve (blue) is the number of photons from the quantum Monte-Carlo simulation of the experiment. It serves for qualitative comparison, is scaled in the vertical direction, and an offset is added to compensate for experimental imperfections. The gray curve shows the full quantum Monte-Carlo simulation for a free-space atom. The error bars in **b** represent one standard deviation and are too small to be visible for some of the data points.

dimensional scan of the detuning  $\Delta_{12}$  against  $\Delta_{23}$ . This scan reveals the complex energy landscape in the first manifold that shows two avoided crossings. The highest photon generation rate is reached on resonance,  $\Delta_{12} = \Delta_{23} = 0$ , with a rate of the order of 100 kHz.

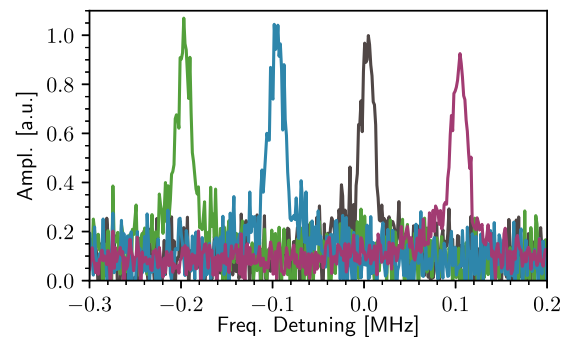
**Excitation-less photon generation.** To demonstrate that these photons stem from transitions between dark states, and therefore do not suffer from atomic decay, the figure of merit is the ratio of photons produced in the cavity per residual atomic excitation. This number is proportional to the total number of photons the system can generate before it decays into an uncoupled state (see Note 4 in the Supplementary Information). Such a channel out of the system is only possible via spontaneous decay from the excited state. To that end, Fig. 3a shows in orange the measured

photon-number probability distribution for a measurement time of  $60 \mu\text{s}$ . In that interval we measure on average 4.0 photons (out of presumably 16 produced photons, due to the limited total detection efficiency of 26%). The gray background curve in Fig. 3a shows the photon number from a quantum simulation of an identical level scheme without a cavity (and therefore no strong coupling). This simulation assumes infinite measurement time and a detector capable of detecting photons in a  $4\pi$  solid angle around the atom (to account for the loss of directionality due to the lack of a cavity), with the same total quantum efficiency as in the experiment. The total expected number of detected photons before this system is pumped into an uncoupled state is then 1.6, which is a factor of 2.5 smaller than our measured result of 4.0 photons.

Extending this result, Fig. 3b plots the average number of measured photons as a function of  $\Delta_{23}$ , extrapolated for infinite measurement times. In the zero-detuning case we find 6.9(1) photons. Comparing this to the cavity-free result of 1.6 photons, our strongly coupled system shows a 4.3-fold increase in the number of photons generated in the more realistic comparison between infinite measurement times. Additionally, a clear peak is seen in the data, demonstrating that the dark state transition occurs exclusively at zero detuning. This contrasts the result of the quantum simulation without a cavity (gray curve in Fig. 3b), which is essentially a flat line at around 1.6 photons. The simulations were done as quantum Monte-Carlo simulations with the full atomic system with additional levels as described in the Supplementary Information (see Note 4 and Figs. S3 and S4). Limitations of this enhancement factor are also discussed in the Supplementary Information (see Note 3 and 5 and Fig. S2).

**Four-wave mixing.** We characterize the generated field with a heterodyne detection setup that is used as a spectrum analyzer as described in the methods section. Different spectra of the newly generated light field are shown in Fig. 4.

The spectral width of the light field is around 20 kHz for a measurement time of  $55 \mu\text{s}$ . This small width can be explained by the fact that all drive lasers, including the local oscillator which is used to measure the spectrum, are phase locked to a common frequency comb that serves as a reference. This measurement thus shows that the newly generated field is phase coherent to all input lasers with a remarkable coherence length. To investigate how the new light field behaves under change of the input light fields, we tune the frequency of these sequentially as seen in the green, blue and violet plot in Fig. 4. When tuning the frequency of the input field, the output field changes its frequency according to



**Fig. 4 Frequency tuning of the new light field.** This shows the spectrum of the cavity output field as measured via a heterodyne setup for different input field detunings. The starting point is the black curve with  $\Delta_{1r} = \Delta_{2r} = \Delta_{23} = 0$ . The other curves are detuned by  $\Delta_{1r} = 100$  kHz for the blue,  $\Delta_{2r} = 100$  kHz for the violet,  $\Delta_{23} = 200$  kHz for the green. The measured amplitude is normalized to the largest amplitude.

$\omega_{\text{fwm}} = \omega_{1r} + \omega_{23} - \omega_{2r}$ , reflecting energy conservation. This shows that the system indeed mediates a nonlinear four-wave-mixing process with one single atom.

**Climbing the ladder of dark states.** To investigate the ladder of dark states in greater detail, it is helpful to derive the interaction Hamiltonian of the system. For all fields being resonant ( $\Delta_{12} = \Delta_{23} = 0$ ), and in the regime  $\Omega_{23} \ll g$  the interaction Hamiltonian simplifies to (with  $\hbar = 1$ )<sup>11</sup>

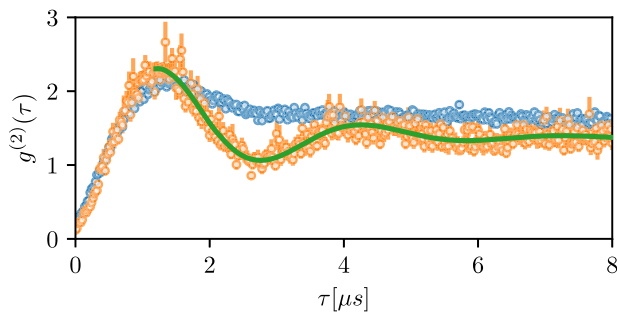
$$H_{\text{int}} \simeq -\frac{\Omega_{12}}{2} |\Psi_1^0\rangle \langle \Psi_0^0| - \sum_{n=1}^{\infty} \frac{\Omega_{12}\Omega_{23}}{4g\sqrt{n}} |\Psi_{n+1}^0\rangle \langle \Psi_n^0| + h.c. \quad (4)$$

For higher  $\Omega_{23}$  this expression becomes lengthy and can be found under Note 2 in the Supplementary Information.

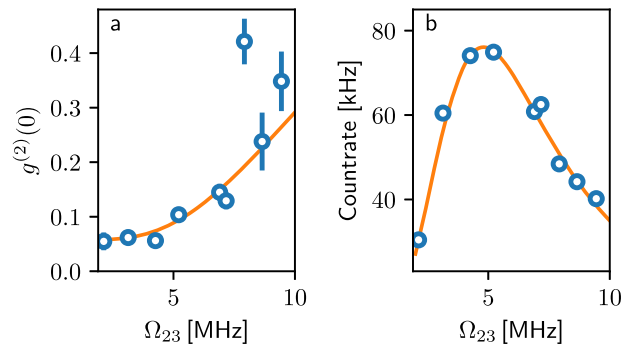
The Hamiltonian in Eq. (4) describes the generation of photons in the cavity mode via transitions between different dark states that avoid exciting the atom. It also shows that although transitions between each pair of subsequent dark states in the ladder are possible, the transition strengths and the decay rates of the dark states (as Fig. 1c shows) change in a highly nonlinear fashion with the excitation rung. In fact, the decrease in driving strength to, along with the increase in decay rate from, the higher-lying dark states, results in a restriction of the Hilbert space to lower photon number states, leading to a quantum Zeno effect<sup>18</sup>. As a result, the system is restricted to the first two dark states, where it behaves like a two-level atom and higher rungs are blocked.

Insights into the dynamics within the ladder of dark states can be obtained by investigating the photon statistics via the standard correlation function  $g^{(2)}(\tau)$ . Measured data for two different values of  $\Omega_{23}$  are shown in Fig. 5. They display strong photon antibunching and pronounced sub-Poissonian statistics. This single-photon characteristic shows that the system indeed exhibits a Zeno blockade as higher dark state rungs are strongly suppressed. Also visible is a damped oscillation with frequency of  $\Omega_{12}/2\pi$ , due to the Rabi oscillation between the lowest dark states  $|\Psi_0^0\rangle$  and  $|\Psi_1^0\rangle$ . The green curve is a fit of a damped oscillation to the data that determines this frequency to 327(14) kHz which is in decent agreement with the calculated frequency of 400 kHz, estimated from the laser powers.

The two curves in Fig. 5 feature the same oscillation frequency and rise time for different  $\Omega_{23}$ , but the decay constant of the oscillation changes, showing that the lifetime of the dark state and



**Fig. 5 Photon correlation function.** Two-photon correlation function measured with two single-photon detectors in Hanbury Brown and Twiss configuration with a coincidence window of 20 ns. Shown are correlation functions for detunings  $\Delta_{12} = \Delta_{23} = 0$  and driving strengths  $\Omega_{23}/2\pi = 2.0$  MHz (orange dots) and  $\Omega_{23}/2\pi = 3.7$  MHz (blue dots). On top of the orange dots is a sinusoidal fit with exponentially decaying amplitude (green line). The error bars represent one standard deviation and are too small to be visible for some of the data points.



**Fig. 6 Zeno blockade.** **a** The equal-time correlation value for different driving strengths  $\Omega_{23}$  for  $\Omega_{12}/2\pi = 300$  kHz. **b** The measured photon rate of the cavity output for the same measurement. The orange lines show a quantum simulation of the simplified system with a position averaged coupling constant of  $g/2\pi = 9.2$  MHz and a (slight) amplitude correction of the photon production rate to accommodate the data. The error bars in **a** and **b** represent one standard deviation and are too small to be visible for some of the data points.

therefore the coherence time depends on  $\Omega_{23}$  (see Fig. 1c and Note 2 in the Supplementary Information for the dark state decay rates). Note that the dephasing rate for the Rabi oscillation differs from the linewidth in Fig. 4. This is not a contradiction as first-order coherence does not imply second-order coherence<sup>19</sup>, and indicates that the individual photons are delocalized in a continuous and coherent wave.

Going beyond the effective two-level system is possible as both the decay rates and the effective driving strength are tunable with  $\Omega_{23}$ . A higher value of  $\Omega_{23}$  allows one to climb the harmonic dark-state ladder and operate the system in a regime where it exhibits a more linear behaviour. In this context, Fig. 6a displays the equal-time photon correlation for increasing  $\Omega_{23}$  and a fixed  $\Omega_{12}$ . It shows that  $g^{(2)}(0)$  increases with  $\Omega_{23}$ ; the system deviates from a two-level system and approaches the photon statistics of a coherent field when the Zeno blockade is removed and higher-lying dark states become populated. Counterintuitively, a stronger control field does not always increase and in fact even decreases the number of emitted photons, as displayed in Fig. 6b. This behaviour is predicted by the full analytic formula for the effective driving strength given in the Supplementary Information (see Note 2 and Fig. S1). It proves that the change of the photon statistics does not simply reflect a buildup of photons in the cavity, but instead is an effect of turning the system into a linear one.

The closed cycling scheme presented here is generic and could be implemented in all strongly coupled cavity systems to suppress emitter excitation. This is particularly relevant, for instance, in the fluorescence observation of molecules, where excitation leads to rapid depumping to uncoupled rovibrational states. In addition to creating more photons, our method has the additional advantage that it provides a background-free signal as the newly generated field is of completely different frequency than the input drivings. Further prospects are opened up by increasing the driving strength  $\Omega_{12}$  between the two ground states. This can result, e.g., in the generation of Schrödinger-cat states of light<sup>11</sup>. Our scheme is also interesting for the investigation of cycles that simulate Hamiltonians from many-body physics under continuous observation<sup>20</sup>. Finally, closed cycles driven by light fields at the single-photon level could offer intriguing possibilities for the realization of quantum heat engines where cavity fields could act as non-classical heat baths along the thermodynamic cycle<sup>21</sup>.

## Methods

The aforementioned experiments are performed with a single  $^{87}\text{Rb}$  atom trapped inside a high finesse resonator using a three-dimensional optical lattice. This leads to typical trapping times of around 6 s during which measurements are taken at a rate of about 1 kHz. A detailed description of the experimental trapping setup and information about the used resonator are given in ref. 22. A typical experimental sequence consists of a cooling interval followed by optical pumping to a specific Zeeman substate (e.g.,  $|1\rangle$  as defined in the results section) and the subsequent experiment.

We investigate the newly generated field in the experiment via two single photon detectors in a Hanbury Brown and Twiss configuration for intensity and correlation measurements or in the spectral domain by heterodyne detection. The heterodyne detection method employs two photodiodes and a strong local oscillator beam (LO) at frequency  $\omega_{\text{LO}}$  that is superimposed with the light field to be measured (called probe; at frequency  $\omega_p$ ), producing an electronic beat signature at frequency  $\omega_b = |\omega_{\text{LO}} - \omega_p|$ . Using this scheme, it is possible to detect light with extremely low power by optical amplification of the probe caused by the LO. In contrast to a homodyne scheme, where  $\omega_{\text{LO}} = \omega_p$ , LO and probe have separate frequencies, thus circumventing detector noise which predominantly occurs at low frequencies. Moreover, using balanced photodiodes we cancel classical intensity fluctuations, making the setup more sensitive. The electronic demodulation process after the output of the balanced photodiodes generates two signals, each of which is proportional to one of the field quadratures of the probe. The demodulation is based on mixing the sinusoidal beat between probe and LO with an electronic local oscillator wave (eLO) at frequency  $\omega_{\text{eLO}}$ . In addition, we implement a low pass filter with cutoff frequency  $\omega_{\text{LP}}$  to remove high frequency noise after the downmixing process. With the two quadrature signals, we can deduce the amplitude and phase of the probe beam. The heterodyne setup is here predominantly used as a spectrum analyzer. When recording a spectrum, we fix  $\omega_{\text{eLO}}$  and vary  $\omega_{\text{LO}}$  with an AOM. A signal can only be observed if the following condition is satisfied:  $|\omega_{\text{eLO}} - \omega_b| < \omega_{\text{LP}}$ . This represents a scanning window which produces a non-zero output signal if the probe frequency  $\omega_p$  lies within the window.

## Data availability

Data is available from the authors upon request.

Received: 7 February 2021; Accepted: 23 February 2021;

Published online: 23 March 2021

## References

- Alzetta, G., Gozzini, A., Moi, L. & Orriols, G. An experimental method for the observation of r.f. transitions and laser beat resonances in oriented Na vapour. *Il Nuovo Cimento B* **36**, 5–20 (1976).
- Harris, S. E., Field, J. E. & Imamoglu, A. Nonlinear optical processes using electromagnetically induced transparency. *Phys. Rev. Lett.* **64**, 1107–1110 (1990).
- Kasapi, A., Jain, M., Yin, G. Y. & Harris, S. E. Electromagnetically induced transparency: propagation dynamics. *Phys. Rev. Lett.* **74**, 2447–2450 (1995).
- Mompart, J. & Corbalán, R. Lasing without inversion. *J. Opt. B* **2**, R7–R24 (2000).
- Kuhn, A., Hennrich, M. & Rempe, G. Deterministic single-photon source for distributed quantum networking. *Phys. Rev. Lett.* **89**, 067901 (2002).
- Specht, H. P. et al. A single-atom quantum memory. *Nature* **473**, 190–193 (2011).
- Ritter, S. et al. An elementary quantum network of single atoms in optical cavities. *Nature* **484**, 195–200 (2012).
- Reiserer, A. & Rempe, G. Cavity-based quantum networks with single atoms and optical photons. *Rev. Modern Phys.* **87**, 1379–1418 (2015).
- Vitanov, N. V., Rangelov, A. A., Shore, B. W. & Bergmann, K. Stimulated Raman adiabatic passage in physics, chemistry, and beyond. *Rev. Modern Phys.* **89**, 015006 (2017).
- Pope, T. J. et al. Coherent trapping in small quantum networks. *J. Stat. Mech.* **2019**, 124024 (2019).
- Villas-Boas, C. J., Tolazzi, K. N., Wang, B., Ianzano, C. & Rempe, G. Continuous generation of quantum light from a single ground-state atom in an optical cavity. *Phys. Rev. Lett.* **124**, 093603 (2020).
- Merriam, A. J. et al. Efficient nonlinear frequency conversion in an all-resonant double-lambda system. *Phys. Rev. Lett.* **84**, 5308–5311 (2000).
- Dubin, F. et al. Quantum to classical transition in a single-ion laser. *Nat. Phys.* **6**, 350–353 (2010).
- Mücke, M. et al. Electromagnetically induced transparency with single atoms in a cavity. *Nature* **465**, 755–758 (2010).
- Kampschulte, T. et al. Optical control of the refractive index of a single atom. *Phys. Rev. Lett.* **105**, 153603 (2010).
- Albert, M., Dantan, A. & Drewsen, M. Cavity electromagnetically induced transparency and all-optical switching using ion Coulomb crystals. *Nat. Photon.* **5**, 633–636 (2011).
- Souza, J. A., Figueroa, E., Chibani, H., Villas-Boas, C. J. & Rempe, G. Coherent control of quantum fluctuations using cavity electromagnetically induced transparency. *Phys. Rev. Lett.* **111**, 113602 (2013).
- Misra, B. & Sudarshan, E. C. G. The Zeno's paradox in quantum theory. *J. Math. Phys.* **18**, 756–763 (1977).
- Höffges, J. T., Baldauf, H. W., Eichler, T., Helmfrid, S. R. & Walther, H. Heterodyne measurement of the fluorescent radiation of a single trapped ion. *Optics Commun.* **133**, 170–174 (1997).
- Laflamme, C., Yang, D. & Zoller, P. Continuous measurement of an atomic current. *Phys. Rev. A* **95**, 043843 (2017).
- Harbola, U., Rahav, S. & Mukamel, S. Quantum heat engines: a thermodynamic analysis of power and efficiency. *EPL (Europhysics Letters)* **99**, 50005 (2012).
- Hansen, C. Interacting Photons in a Strongly Coupled Atom-Cavity System. Dissertation, Technische Universität München, München (2017).

## Acknowledgements

B.W. was supported by Elitenetzwerk Bayern (ENB) through the doctoral program ExQM. K.N.T. was supported by the Deutsche Forschungsgemeinschaft (DFG) under Germany's Excellence Strategy - EXC-2111 - 390814868. C.J.V.-B. thanks the support by the Sao Paulo Research Foundation (FAPESP) Grants No. 2018/22402-7 and No. 2019/11999-5, and National Council for Scientific and Technological Development (CNPq) Grants No. 307077/2018-7 and No. 465469/2014-0.

## Author contributions

All of the authors (K.N.T., B.W., C.I., J.N., C.J. V.-B. and G.R.) contributed to the theoretical understanding, the analysis of the measurements and the writing of the manuscript.

## Funding

Open Access funding enabled and organized by Projekt DEAL.

## Competing interests

The authors declare no competing interests.

## Additional information

**Supplementary information** The online version contains supplementary material available at <https://doi.org/10.1038/s42005-021-00559-7>.

**Correspondence** and requests for materials should be addressed to K.N.T.

**Reprints and permission information** is available at <http://www.nature.com/reprints>

**Publisher's note** Springer Nature remains neutral with regard to jurisdictional claims in published maps and institutional affiliations.



**Open Access** This article is licensed under a Creative Commons

Attribution 4.0 International License, which permits use, sharing, adaptation, distribution and reproduction in any medium or format, as long as you give appropriate credit to the original author(s) and the source, provide a link to the Creative Commons license, and indicate if changes were made. The images or other third party material in this article are included in the article's Creative Commons license, unless indicated otherwise in a credit line to the material. If material is not included in the article's Creative Commons license and your intended use is not permitted by statutory regulation or exceeds the permitted use, you will need to obtain permission directly from the copyright holder. To view a copy of this license, visit <http://creativecommons.org/licenses/by/4.0/>.

© The Author(s) 2021